

Article

Spatial Variations of Deformation along a Strike-Slip Fault: A Case Study of Xianshuihe Fault Zone, Southwest China

Jinxuan Li ^{1,2}, Songfeng Guo ^{1,3,4,*} , Shengwen Qi ^{1,3,4} , Qianhui Wei ^{1,5}, Bowen Zheng ^{1,3,4}, Yu Zou ^{1,3,4}, Yongchao Li ^{1,3,4}, Yaguo Zhang ² and Xiao Lu ^{1,3,4}

- ¹ Key Laboratory of Shale Gas and Geoenvironment, Institute of Geology and Geophysics, Chinese Academy of Sciences, Beijing 100029, China; lijinxuan0703@163.com (J.L.); qishengwen@mail.iggcas.ac.cn (S.Q.); z20211020254@stu.ncwu.edu.cn (Q.W.); zhengbowen@mail.iggcas.ac.cn (B.Z.); zouyu@mail.iggcas.ac.cn (Y.Z.); liyongchao@mail.iggcas.ac.cn (Y.L.); luxiao@mail.iggcas.ac.cn (X.L.)
- ² School of Civil Engineering, Chang'an University, Xi'an 710061, China; zhangyaguo29@163.com
- ³ Innovation Academy of Earth Science, Chinese Academy of Sciences, Beijing 100029, China
- ⁴ University of Chinese Academy of Sciences, Beijing 100049, China
- ⁵ College of Geosciences and Engineering, North China University of Water Resources and Electric Power, Zhengzhou 450046, China
- * Correspondence: guosongfeng@mail.iggcas.ac.cn

Abstract: The distribution of damage zones around a fault has long been regarded as a frontier and hot spot in the field of geoscience but is still not fully understood. In this study, we conducted field investigations and tests around the Xianshuihe fault zone (XSHF), a left-lateral strike-slip fault with a length of about 400 km located in the eastern margin of the Tibetan Plateau. The results reveal that the fracture frequency and rock strength parameters present a spatially asymmetric distribution along the fault and have a negative power-law correlation with the distance from the fault. The widths of the damage zones are approximately 20.8 km and 17.1 km in the southwest and northeast directions, respectively. Combined with the previous studies, we presented a negative power-law function to depict the correlation between slip displacement and the width of the damage zone and found that the growth rate of damage zone in faults with low displacement is greater than that in those with large displacement. The study demonstrates that the asymmetric distribution of the damage zone surrounding the XSHF is mainly due to the stress redistribution in different damage zones stemming from the left echelon and different activity rates of the blocks on both sides of the XSHF.

Keywords: Xianshuihe fault zone; strike-slip fault; damage zone; fracture frequency; rock strength



Citation: Li, J.; Guo, S.; Qi, S.; Wei, Q.; Zheng, B.; Zou, Y.; Li, Y.; Zhang, Y.; Lu, X. Spatial Variations of Deformation along a Strike-Slip Fault: A Case Study of Xianshuihe Fault Zone, Southwest China. *Appl. Sci.* **2024**, *14*, 2439. <https://doi.org/10.3390/app14062439>

Academic Editor: Eduardo Ferreira da Silva

Received: 5 February 2024

Revised: 5 March 2024

Accepted: 9 March 2024

Published: 14 March 2024



Copyright: © 2024 by the authors. Licensee MDPI, Basel, Switzerland. This article is an open access article distributed under the terms and conditions of the Creative Commons Attribution (CC BY) license (<https://creativecommons.org/licenses/by/4.0/>).

1. Introduction

Fault zones are generally considered to have a bunch of shear zones characterized by tectonically damaged rock fabrics [1]. The damage zones here refer to the highly deformed area on both sides of the main fault [2,3]. Based on position, the damage zones associated with a geologic fault can be classified either as fault tip damage zones, fault wall damage zones, and fault linking damage zones or damage zones along-fault, damage zones around the fault tip, and cross-fault damage zones [4]. Additionally, based on the kinematic and geometric interaction of the fault, the associated damage zones have been further divided into fault-approaching damage zones and fault-intersecting damage zones [5]. The mechanical characteristics of the rock and the regional strain distribution can be greatly influenced by fault damage zones [6,7]. Therefore, identifying the width and distribution pattern of fault damage zones is essential for recognizing some very important aspects, i.e., the regional tectonic evolution [8,9], seismic characteristics [10,11], crustal fluid permeability [3,12], subsurface sequestration of CO₂ [13,14], and distribution of the ground stress field [15,16].

The developmental characteristics of fault damage zones have been the subject of many studies over the past decades. These previous studies include the structural characterization

of damage zones based on geologic maps, field surveys, and microstructural analyses of orientated rock samples [2,17], as well as the characterization of the damage zone evolution associated with geologic faults, based on numerical models and diagenetic environments [11,18,19]. In general, determining the width of the fault damage zone is crucial. It is usually defined by the distribution and frequency of the cracks, fractures, and deformation zones of the damaged structures, which normally decreases with increasing distance from the main fault core [20]. For quantitatively portraying the width of fault damage zones, some scholars carried out studies on the scalar correlations between the width and displacement of fault damage zones based on fault evolution models [21], while others studied the distribution pattern of the damage zones based on the statistical evaluation of the fracture frequency at a distance from the fault zone [22,23].

There often exists a close correlation between the width of the damage zones and the cumulative displacement of the fault, but it is still relatively difficult to accurately quantify the extent of width of the damage zones associated with an active fault because the physical and mechanical characteristics of the rock in the damage zones change progressively away from the core of the main fault [24,25]. Most of the studies regarding the determination of the width of the fault damage zones targeted small-scale faults [4,23], and knowledge of the rock damage conditions surrounding large-scale active fault zones is still absent, especially when they have a length of more than 100 km. However, large-scale fault zones, which usually act as boundary faults between lithospheric plates, have a significant impact on the control of the regional crustal stress–deformation field and profoundly influence seismic activities [26,27]. The development of the damage zones around such large geologic faults is closely related to the regional geomorphic evolution and mountain hazards [28,29] in that area. Since the 21st century, many major strategic projects have been proposed in southwest China; therefore, for safe and resilient construction of these projects, prior determination of the width of the damage zones along major faults is a crucial activity.

For this study, we selected the Xianshuihe fault zone (XSHF) in the eastern margin of the Qinghai–Tibet Plateau (Figure 1a) [30]. In the Cenozoic, the Tibetan Plateau uplifted and its materials moved and extruded eastward. As a result, the Mesozoic structures in the western margin of the Yangtze block were superimposed and transformed into large-scale strike-slip faults and thrusts [31,32], and the XSHF is one of the most active faults and serves as the eastern boundary of the Qinghai–Tibet Plateau; it also has unique intracontinental deformation characteristics [33]. The XSHF is a prominent arc-linear, northwestern–southeastern trending fault. In the vicinity of the Huiyuan temple basin, the XSHF can be divided into northwestern and southeastern segments. The northwestern segment of the XSHF is characterized by a left echelon pattern, while in the southeastern section, four secondary sub-faults diverged through the Huiyuan temple basin and eventually developed southward in Kangding, where XSHF splays coincided. In Shimian, the splays of the XSHF are connected with the Anninghe fault zone and the Daliangshan fault zone, forming the west boundary of the “Y” structural belt and the northeastern (NE) boundary of the Sichuan–Yunnan block, as well as the southern boundary of the Bayan Har block [27,30]. The XSHF plays an important role in accommodating late Cenozoic crustal deformation of the eastern Tibetan Plateau [27,34], where there is a drop in elevation from the western Sichuan Plateau (4.5–5 km) to less than 1 km in the Sichuan Basin within a distance of 50–200 km [35]. Other studies regarding the tectonic uplift of the eastern margin of the Qinghai–Tibet Plateau have also demonstrated the indelible role of the XSHZ [35–37]. Due to block interactions, many destructive earthquakes have occurred along the XSHF [38,39], including the 1923 Daofu earthquake (M7.3), 1955 Kangding Earthquake (M7.5), and 1973 Luhuo Earthquake (M7.9), etc., (Figure 1b).

Therefore, we attempt to quantitatively characterize the development of the rock damage parameters in different parts of the XSHF zone through extensive field investigations. In this study, we combine the detailed acquired data and analysis for identification of the width of the damage zones under multifactorial perturbation and to quantitatively evaluate the quality of engineered rocks. Finally, we discuss the influence of the tectonic activity

and stress field on the development of these damage zones along the XSHF. This detailed study is intended to provide a reference for understanding the development pattern of the damage zones of large-scale active faults and for selecting suitable sites for ongoing as well as proposed major projects in the region.

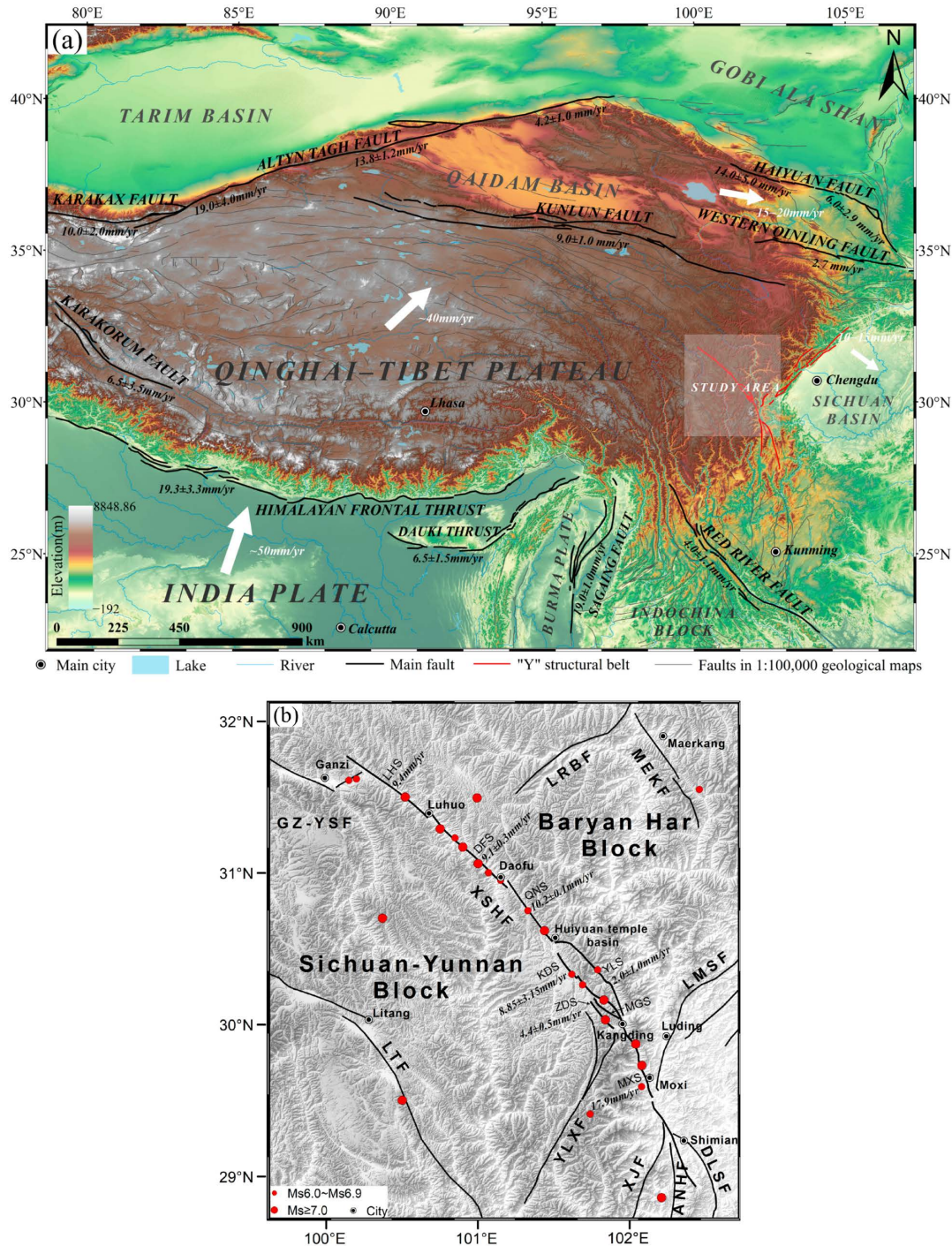


Figure 1. (a). Topography and principal active faults of Qinghai–Tibet plateau and adjacent regions. White arrows indicate motions of India, central Tibet, northeastern most Tibet, and Sichuan relative to Siberia (modified after Tapponnier, et al., 2001 [37], based on the Geographic Coordinate System—GCS_WGS_1984, DEM (Digital Elevation Model) data from ASF Data Search (alaska.edu)); (b). Spatial distribution and seismic development of XSHF; historical earthquake data are from Wen et al., 2008 [39] and China Earthquake Network (<http://www.ceic.ac.cn>). (XSHF—Xianshuihe fault

zone, GZ-YSF—Ganzi–Yushu fault zone, XJF—Xiaojiang fault zone, ANHF—Anninghe fault zone, DLSF—Daliangshan fault zone, LTF—Litang fault zone, LRBF—Longriba fault zone, MEKF—Maerkang fault, YLXF—Yulongxi fault zone, LMSF—Longmenshan fault zone; LHS—Luhuo segment, DFS—Daofu segment, QNS—Qianning segment, KDS—Selaha–Kangding segment, YLS—Yalahe segment, ZDS—Zheduotang segment, MGS—Mugecuo segment, MXS—Moxi segment).

2. Materials and Methods

2.1. Geological Setting

The XSHF has been one of the most active strike-slip faults in the eastern margin of the Qinghai-Tibet Plateau since the Cenozoic [27]; it is slightly arc-shaped towards the northeast, with a total length of approximately 400 km, a strike of 40°–50° NW, and a dip of 55°–80° [40]. The XSHF can generally be divided into northwestern (NW) and southeastern (SE) segments using the Huiyuan Temple Basin. The NW segment is developed in a slightly overlapping left-stepped echelon and can be divided into three segments from northwest to southeast: the Luhuo segment (LHS), Daofu segment (DFS), and Qianning segment (QNS). The SE segments diverge through the Huiyuan Temple Basin to form multiple secondary faults, i.e., the Zheduotang segment (ZDS), Selaha–Kangding segment (KDS), and Yalahe segment (YLS); the fault trace overlaps with the Moxi segment (MXS) in the Kangding area and connects with the Anninghehe and Daliangshan fault zones near Shimian County (Figure 1b), forming a large strike-slip fault system. The XSHF divides the Songpan–Ganzi terrane into two, the Bayan Har block to the northeast and the Sichuan–Yunnan block to the southwest, with nearly 80–100 km of left-lateral slip displacement [27,41]. As the northern boundary fault, the XSHF coordinates the extrusion and deformation of the Bayan Har block and Sichuan–Yunnan block.

2.2. Data Source

The characteristics of fracture frequency and rock strength can be significantly affected by faults within a certain width [42]. The consistencies of the fracture frequencies and rock strengths in different parts of the damage zones along a fault are still somewhat controversial. Some studies in this regard have pointed out that variations exist in the degree of fracture frequency and rock strength in different damage zones along a fault [1,4], whereas others are of the opinion that for the same distance from the fault, the width of the damage zones would be relatively consistent [29].

In order to further characterize the spatial distribution of the rock's properties in the damage zones, we conducted a field survey along five NE-directed profiles, with a focus on the intersection area of the secondary faults. All five profiles traverse the XSHF zones in detail and provide good tectonic and bedrock exposures for study (Figure 2a). Considering the activity of the XSHF, its geometric spreading, strain field, and displacement field are spatially distributed with a somewhat non-uniform pattern [43,44], we believe that the width of the damage zones in different parts of the XSHF may not be consistent. To study three different types of damage zones, one tip damage zone (TDZ), one wall damage zone (WDZ), and three linking damage zones (LDZ) were identified in different parts of the XSHF (Figure 2b).

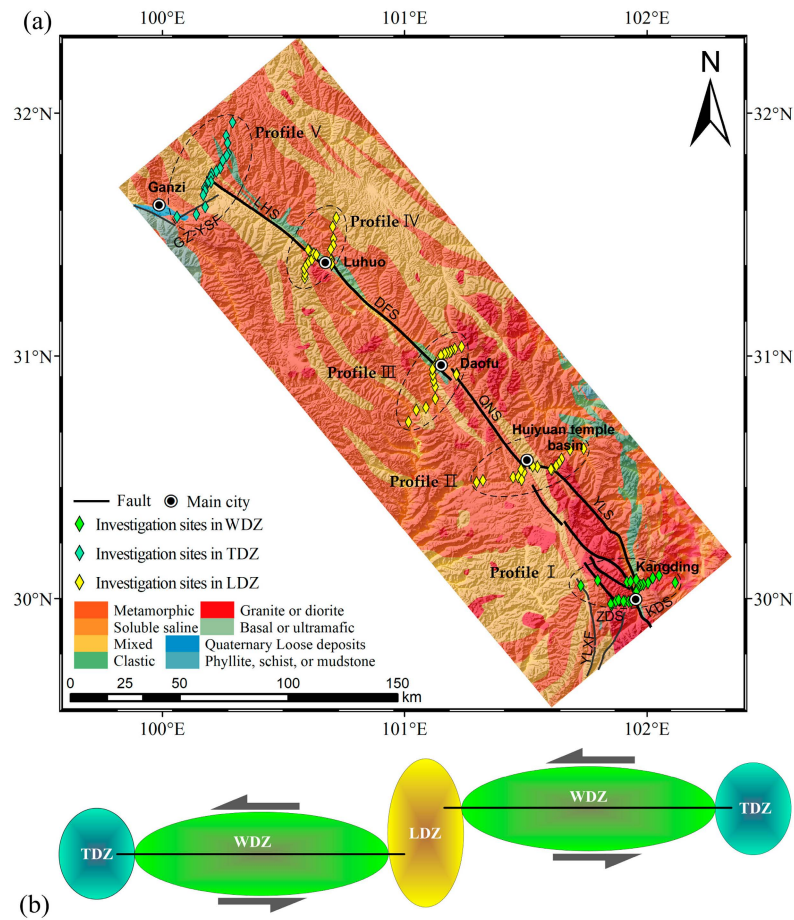


Figure 2. (a). Locations of the investigation sites and geological map of XS HF (the geological data are from the engineering geological petrofabric database [45]); (b). Simple 2D schematic illustration of the fault damage zones around a segmented left-lateral fault (modified after Kim et al. 2004 [1]).

2.3. Characterization of Fracture and Strength Characteristics

In each profile that is generally perpendicular to the strike of the XS HF, point observations were taken at unequal intervals, with shorter intervals closer to the fault walls and longer intervals away from fault walls. These observations were made on both sides of the fault while taking the fault core as the central axis (Figure 2a). The precise geographic coordinates, topographic features, lithologic features, and structural features of the rock were recorded for each point.

Understanding the fracture frequencies of rock mass in the damage zones along geological faults is an essential parameter for quantifying their geometric characteristics [46]. Therefore, three-dimensional geomechanical data has been employed to estimate the fracture frequency (J_v) in the damage zones along each profile (Equation (1)) [47]. We characterized the spatial degree of deformation on both walls of the fault and found that a negative power-law function can well fit the rock fracture frequency at different locations from both walls of the fault (Equation (2)) because the stress generated from the line or point source showed a tendency of power-law decay [48]. During the field survey, the in situ strengths of the bedrock on both sides of the XS HF were measured using the Schmidt hammer rebound test [49].

$$J_v = \sum_{i=1}^n \frac{1}{S_i} \quad (1)$$

$$D = ax^{-n} \quad (2)$$

where S_i is the mean fracture frequency for each surveying site, D is the fracture frequency (m^3), x is the distance from the fault (km), a is a constant, and n is the decay parameter,

which characterizes the degree of decay of the fracture frequency in the damage zones; a larger decay parameter indicates that the damage is attenuated more rapidly [50].

3. Results

3.1. Tip Damaged Zones

The tip damage zone (TDZ) of the XSHF (profile V) is located within the sandstone rock (Figure 2a, Table S1). In the NE wall of the fault, there is fractured sandstone and interbedded slate layer at 4.7 km that becomes blocky at 17.1 km (Figure 3b,d). Within the range of approximately 1.1–2.5 km near the LHS, the fracture frequency is 55–70 per cubic meter; moving away from the LHS, the fracture frequency of the rock gradually decreases to approximately 10–20 fractures per cubic meter between 17.1 and 19.5 km, while the in situ strength of the rock mass in the same region was restored from 28.68 ± 4.26 MPa (within 1.1–2.5 km from the fault) to 47.78 ± 4.03 (within 17.1–19.3 km from the fault) (Figure 4c). The rocks of the southwestern (SW) wall show large fracture frequencies and steep dipping, mostly between 6.6 km and 20.8 km (Figure 3a,c); the distribution of the fracture frequency shows a wave-like trend, decreasing from about 60–90 per cubic meter in the range of 0.2–1.5 km near the fault to 25 per cubic meter at about 10.3 km from the LHS. At 15.1 km from the LHS, due to the influence of the GZ-YSF, the fracture frequency increases sharply to 90 per cubic meter and then develops to the southwest, decreases to 45 per cubic meter gradually, and the in situ strengths of the rock mass have the same characteristics within the SW wall of the LHS, increasing from 28.90 ± 4.03 MPa near the fault (within 0.2~1.5 km from the LHS) to 44.25 ± 2.19 MPa (10.3 km from the LHS), then decreasing to 15.25 ± 1.27 MPa (15.1 km from the LHS), and finally recovering to 27.20 ± 3.93 MPa (Figure 4c).

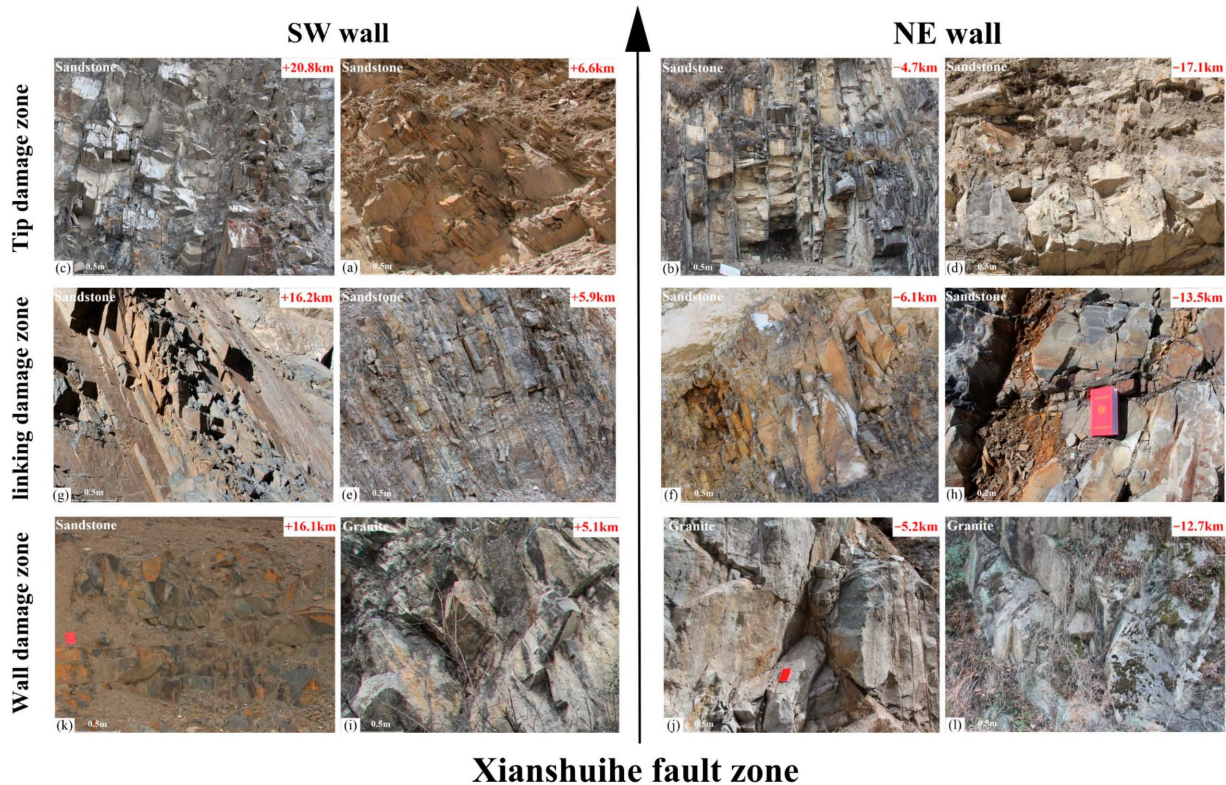


Figure 3. Exposure of bedrock at different positions of two walls in the XSHF.

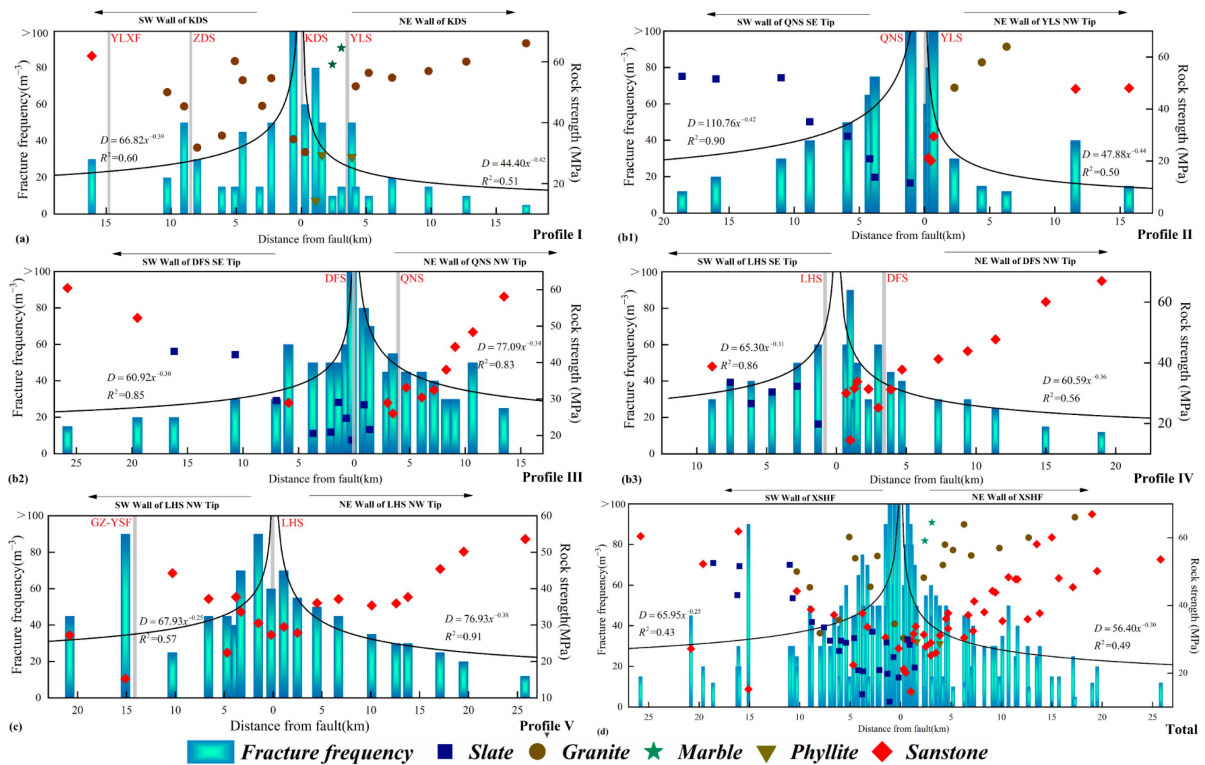


Figure 4. Fault damage zone distributions (strike-slip fracture frequency as bar diagrams against distance from the fault core at each profile).

3.2. Linking Damaged Zones

The linking damage zone (LDZ) of the XSHF (i.e., profiles II, III, and IV) is widely found in rock assemblages like the meta-sandstone and slate formed by the low-grade metamorphism of siltstone (Figure 2a, Tables S2–S4). During the field survey and measurements along profile III at 5.9 km from the DFS on the SW wall, a sufficient quantity of weathered products was observed in the rock mass; as an example, a large amount of weathered denudation detritus exists in the rock mass. The structural planes of the rock strata at the mentioned location are also generally open, with gaps ranging from 1–3 mm and a fracture frequency of 50 to 60 per cubic meter (Figure 3e). At a distance of 16.2 km from the DFS, the exposed bedrock presents a relatively complete block, returning to the undamaged zone with a significant decrease in fracture frequency to 20 per cubic meter (Figure 3g). In the NE wall, the sandstone at 6.1 km and 13.5 km from DFS is also fractured (Figure 3f,h), and the fracture frequency gradually decreased from 70–80 per cubic meter within the range of 0.9–1.4 km near the fault to 25 per cubic meter at 13.5 km, maintaining a high joint density.

The in situ strength of the bedrock shows an obvious “V” distribution across the faults, reaching the valley of the “V” in the fault-connected area, i.e., between the DFS and the QNS, where the compressive strength measured by Schmidt hammer rebound test is about 26.24 ± 5.14 MPa. As it moves away from the DFS, it reaches about 19.5 km and 13.5 km from the SW wall and NE wall of the DFS, respectively, recovered to about 56.35 ± 4.79 MPa and 58.10 ± 5.68 MPa at about 19.5 km and 13.5 km, respectively (Figure 4b,c).

3.3. Wall Damaged Zones

The wall damage zone (WDZ) of the XSHF is found within the Zheduoshan granitoid and traversed by profile I (Figure 2a, Table S5). Due to the active tectonic movements in the study area, the “X” joints in the granitic rocks exhibit an opening of about 1–2 cm at a distance of 5 km from both the walls of the KDS. These openings were found filled with large amounts of detritus material (Figure 3i,j). As we move away from the faults, the

sandstone outcrop in the SW wall, at about 16.1 km, is still characterized by a cataclastic texture (Figure 3k). On the other hand, the rock mass is not very jointed, and the joints are tightly closed at about 12.7 km in the NE wall (Figure 3l).

The fracture frequency generally shows a clear trend of gradual decrease as we move away from the fault core. On the SW wall, the fracture frequency decreased from over 100 per cubic meter (0.6 km from the segment KDS) to 12–15 per cubic meter (within 5.1–6.1 km from the KDS) and then increased to 30–50 per cubic meter near the ZDS. As the fracture zones continue to move away from the KDS and are affected by YLXF, the fracture frequency is generally high, exceeding 20–30 per cubic meter. Similarly, on the NE wall, the fracture frequency decreases from 65–80 per cubic meter (within 0.3–1.1 km from the KDS) to 5–15 per cubic meter (within 2.4–3.1 km from the KDS) and then increases to 20–60 per cubic meter near the YLS (within 3.9–4.2 km from the KDS); however, as the fracture zones move away from the YLS, the fracture frequency rapidly decreases to 10–15 per cubic meter within the range of 9.8–12.7 km (Figure 4a). The in situ strength of the exposed bedrock reveals a nearly “W”-shaped distribution with the distance from the fault. The ZDS and KDS-YLS are at the bottom of the “W” valley, with magnitudes of 31.64 ± 5.74 MPa and 37.70 ± 18.44 MPa, respectively. However, the in situ strength of the exposed bedrock between the ZDS and KDS (5.1 km away from the KDS), as well as away from the fault (approximately 12.7 and 16.1 km from the NE and SW wall, respectively), reaches “W” shaped peaks, with magnitudes of 60.20 ± 8.80 MPa, 60.40 ± 5.02 MPa, and 61.90 ± 3.38 MPa, respectively.

4. Discussion

4.1. Determination of Damage Zone

The statistical results indicate that the fracture frequency and rock strength on both walls of the XSHF hold an obvious relationship with the distance from the fault core (Figure 4). By observing the rock outcrops in the field, power-law function fitting, and comparing the rock properties in the damage zones with the rocks of the same type but undeformed (protolith zone) [50,51], we can determine the extents and boundaries of the different types of damage zones associated with the XSHF (Table 1). When the fracture frequency of the rock mass is less than or equal to 20–30 fractures per cubic meter, such rock mass would be considered outside of the actual fault zone.

Table 1. The boundary of the damage zones of XSHF.

	Profile ID	SW Wall		NE Wall	
		Width (km)	<i>n</i>	Width (km)	<i>n</i>
Wall damage zone	I	16.1	0.39	12.7	0.42
	II	16	0.42	15.7	0.44
Linking damage zones	III	16.2	0.30	13.5	0.34
	IV	>8.9	0.31	15	0.36
Tip damage zone	V	≥20.8	0.25	17.1	0.38
Total		≥20.8	0.335 ± 0.085	17.1	0.39 ± 0.05

In the TDZ (Profile V), the inclination of the rock on the NE wall within the range of 0–17.1 km changes from steep to gentle and the completeness of the rock mass changes from fragmented to blocky, indicating that the level of tectonic activity on the NE wall of the LHS has significantly decreased within the range. On the SW wall, due to the superimposed disturbance of the GZ-YSF and LHS, the fracture frequency has remained at a relatively high level within a distance of 20.8 km from the LHS (Figure 4c), and the rock is also fragmented (Figure 3a,c). Therefore, we believe that the boundary of the fracture zone on the SW wall of the XSHF tip is at about 20.8 km (Table 1). The damage zone boundary associated with the LDZ is more uniform, the fracture frequency decreased to less than 20 per cubic meter at distances of 16.1 ± 0.1 km (Figure 4(b1,b2)) and 14.6 ± 1.1 km (Figure 4(b1,b3)) from the SW wall and NE wall, respectively (Table 1). On both walls of WDZ, there is a composite

disturbance of ZDS and YLS (Figure 2a), but the distance between the NE boundary and the KDS is 12.7 km, which is less than the 16.1 km of the SW wall (Table 1). This seems to indicate that the different damage widths of the two walls are affected by the fault activity, as the activity rate of the YLS is 1.05 ± 0.45 mm/yr [52], which is smaller than that of ZDS, which is 4.1 ± 0.7 mm/yr [53].

We can see that there are obvious differences in the widths of different damage zones and damage zones in the two walls of the XSHF, i.e., TDZ > LDZ > WDZ and SW wall > NE wall (Table 1). Previous studies have indicated that the asymmetry of the damage zone may include the deformation history [54,55], geometrical spreading [4], seismic rupture [56], stratigraphic lithology [57], and so on. Considering the difficulty in calculating the surface rupture caused by frequent earthquakes along the XSHF, as well as the fact that the lithology of hard rocks such as sandstone and granite is relatively single, we discussed the differential distribution of the damage zones of the XSHF caused by stress distribution and fault activity.

4.2. The Characterization of Rock Damage Distribution

4.2.1. Characteristics of Rock Damage Density Decay

Damage zones result from the initiation, propagation, interaction, and build-up of slip along faults [1]. These fault damage zones can be influenced by factors such as fault length, displacement, deformation history, and rock mechanical properties [58]. Based on the power-law fitting of the fracture frequency in the study area, we found that the intensity of the damage decay of the rocks in the two walls, as well as in other different damage zones along the XSHF, is not consistent. Slower damage decay has been observed in the three different damage zones of the SW wall, with decay parameters of 0.39, 0.34 ± 0.09 , and 0.25. In comparison, the largest decay parameter of the WDZ, the middle of the LDZ, and the smallest of the TDZ are presented (Table 1 and Figure 5a).

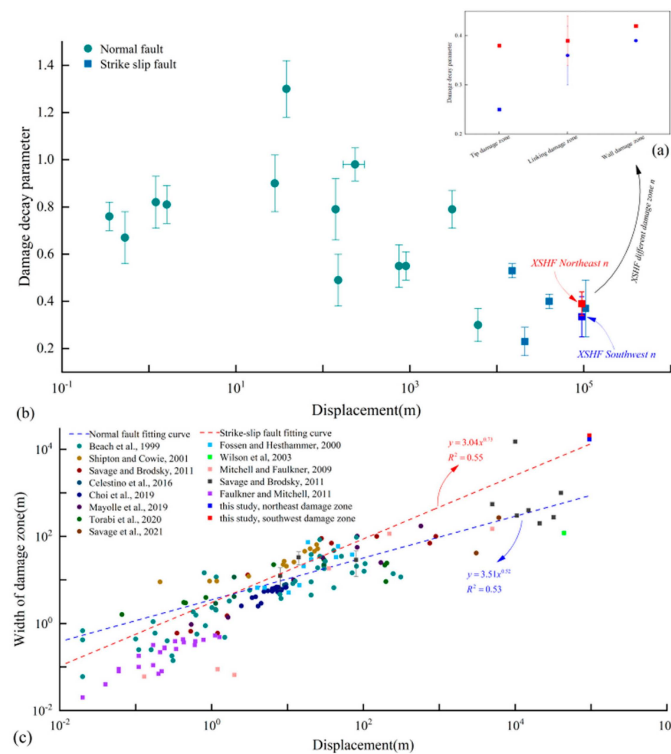


Figure 5. (a) Damage decay parameters of different damage zones in the XSHF; (b) Trends of damage decay parameters with displacement (modified after Savage and Brodsky (2011) [59], Savage et al. (2021) [50]); (c) Distributions of the width of the damage zones in normal faults and strike-slip faults with the cumulative slip on the faults (expressed in logarithmic form, normal faults and strike faults are represented by circles and squares; the blue and red dashed lines represent the fitting curves for the width of damage zone of normal and strike slip faults) [4,9,23,50,54,59–65].

By comparing the damage decay parameters collected during the field survey from the damage zones of the two walls of the XSHF with the data compiled by Savage and Brodsky (2011), we found that it is very similar to other strike-slip faults, i.e., it experienced the same amount of displacement (Figure 5b). In order to fully understand and further clarify the relationship between rock damage decay and the rate of fault displacement, we compared numerous published data [50,59] with the findings of this study. Subsequently, we found that the fault displacement has a significant impact on the damage decay in the rock mass associated with different types of faults. The damage decay parameter of small-displacement faults is much stronger than that of large-displacement faults. As displacement increases, the damage decay parameter “*n*” follows a single hump distribution and is positively correlated with displacements of less than hundreds of meters. However, when fault displacements further increase, the damage decay parameter decreases gradually, i.e., for displacements in the order of 10^4 m or larger, they seem to reach a threshold of about 0.3, indicating a consistent damage decay parameter for large-displacement faults.

4.2.2. Width of the Fault Damage Zones

Combined with the previous studies, we found a power-law relation can depict the relationship between them, even when the slip displacement reaches 100 km and the gap in the damage zone widths can be up to $10^2\sim 10^4$ m or the slip displacement is less than 10^{-1} m (Figure 5c). The power indices of 0.52 and 0.73 for normal faults and strike-slip faults, respectively, are both less than 1, indicating that the development width of fault damage zones slows down with the continuous increase in fault displacement. Previous studies have shown that the threshold for this low displacement is approximately 2×10^3 m [50]. When the cumulative displacement is below this threshold, the rate of increase in the width of fault damage zones becomes more severe with the increase in displacement. That is, low-displacement faults have a larger proportion of damage zones compared to their displacement, possibly because the damage zone in low-displacement faults increases linearly with the displacement at certain locations [54] or only significantly increases during the early sliding period of the fault [66]. By contrast, large-displacement faults with cumulative displacements exceeding 2×10^3 m need to dissipate more energy to become wider as fault slip increases, generating wider zones of damage in the surrounding rock [67]. The significant difference in the width of the damage zones between normal faults and strike-slip faults may be due to the different fault movement types. The damage caused by the compressive stress state in the strike-slip fault is generally stronger than that in the normal fault in the tensile stress state.

4.3. Asymmetry of the Damage Zone

4.3.1. Differences in Damage Zones Due to Stress Distribution

Mechanical test results have shown that the size and angle of the pre-existing fractures in rock samples significantly control the development of microfractures [68,69], because the size and angle of the mentioned fractures in the rock samples greatly affect the stress distribution pattern around the specimen during testing [70–72]. Similar variations in stress distribution can also occur around active fault zones due to differences in the geometric spreading of faults. It is well known that when all other factors are kept constant and only different stress states are considered, the deformation characteristics of the rocks in the damage zones remain constant [73,74]. Therefore, to understand the phenomena behind the development of the rock damage pattern in different zones of the fault, we analyzed the stress field distribution characteristics in different parts of the fault using simple numerical models. In these models, we restrict the displacement of the model in all directions except the applied load direction and kept the mechanical parameters, fault lengths, load magnitudes, etc., the same in all models (Table 2). The simulation results revealed that the angle (α) between the regional far-field principal stress orientation and the fault strike significantly controls the stress distribution characteristics around the

fault (Figure 6e). Stress concentration zones form at the tips of isolated faults and at fault junctions, whereas stress relaxation occurs at the fault walls (Figure 6).

When the α increases from 0 to 90° for an isolated fault, both the magnitude and stress disturbance area increase sharply at the fault tips. The stress disturbance area increases while the magnitude decreases on the two sides of the fault wall (Figure 6(a1–d1)). We performed similar numerical simulations for two neighboring faults. The stress magnitude in the linking damage zone is higher than that at the tip, regardless of if faults are underlapping or adjacent (Figure 6(a2–d2), Figure 6(a3–d3)). However, this relationship becomes reversed when the two faults partially overlap, with a stronger stress concentration at the fault tip damage zone compared to the linking damage zone formed by the fault overlap (Figure 6(a4–d4)). This explains why the width of the TDZ of the XSHF is larger than that of the LDZ. The clockwise rotation of the NNW-NWW in the Sichuan–Yunnan block maintains a small angle with the strike of the XSHF (Figure 6e), resulting in the spatial spreading of the left echelon pattern, with slight overlaps of the XSHF in the region where the regional stress field is similar to that in the generalized Figure 6(b4). However, the WDZ is always in a low-stress zone and is lower than the stress zone in the TDZ or LDZ. We believe that the damage driven by the wide-area stress concentration in the TDZ or LDZ is more intense than that caused by fault slip in the WDZ, which may be an important reason for the difference in damage widths in different damage zones along the XSHF, i.e., the width of the damage in the TDZ or LDZ is wider than that in the WDZ.

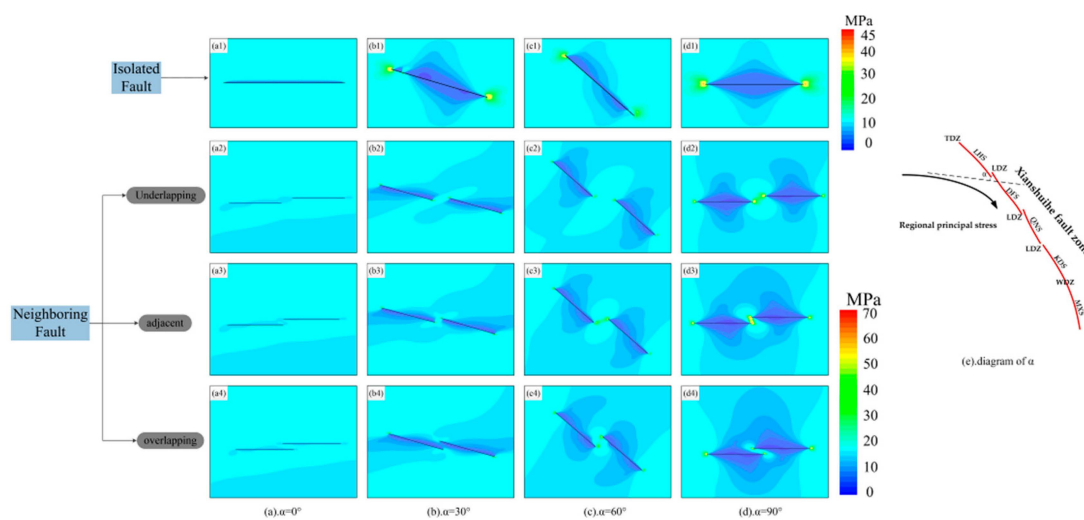


Figure 6. Two-dimensional numerical simulation of faults with different strikes and composite forms: the stress magnitude of an isolated fault between 0 and 45 MPa and the stress magnitude of two neighboring faults between 0 and 70 MPa ((a) regional principal compressive stress at 0° to the fault strike; (b) 30°; (c) 60°; (d) 90°; (e) Schematic diagram of the orientation of regional principal stress at an angle α to the fault strike; the regional principal stress comes from the clockwise rotation of the Sichuan–Yunnan block).

Table 2. Mechanical parameters of the model.

	Poisson's Ratio	Elasticity Modulus (GPa)	Shear Stiffness (GPa)	Normal Stiffness (GPa)	Cohesion (kPa)	Friction Angle (°)
Rock	0.25	25.0	—	—	—	—
Fault zone	—	—	2	2	100	15

4.3.2. Driving Wall Effect in Strike-Slip Faults

Previous studies have shown that the hanging walls of dip-slip faults generally suffer more damage than the footwalls, although the stress state and damage mode of the hanging walls and foot walls are not the same [75,76]. In contrast, when it comes to strike-slip faults, the widths of the surface ruptures in both walls suggest that the damage should be distributed roughly symmetrically all along the fault core [23,77]. However, based on our field investigations and data analysis, we found that the damage zones of the two walls of the XSHF are asymmetrically developed. The width of the damage zone of the SW wall is obviously wider than that of the NE wall (Figure 4, Table 1). One of the most important reasons behind the differential distribution of the damage zones across the XSHF may be due to the fact that the SW wall is a strike-slip driving wall. It is well known that fault slip begins with the loading of plate tectonic motion, and the direction of slip depends on the angle of oblique convergence of the plates and the direction of relative motion with respect to another plate [78]. The active Holocene left-lateral slip of the XSHF suggests that it was significantly controlled by the NE-trending extrusion and collision of the Indian Plate against the Eurasian Plate (Figure 1a). The current studies indicate that the slip rate of the XSHF gradually increased from NW to SE [43,44], with a significant velocity difference between the two walls of the fault. This further suggests that the Sichuan–Yunnan block on the SW wall is less constrained than the Bayan Har block on the NE wall. The eastward movement of the Bayan Har block is absorbed by the high shrinkage rate and strong crustal compression caused by the LMSF, which shortens the crust [79,80], whereas the clockwise rotation of the Sichuan–Yunnan block continues to extend into the north–south oriented fracture system [27]. This tectonic environment and the crustal kinematics have made the XSHF a large-scale left-lateral strike-slip fault to accommodate the different movement rates between the Chuan–Dian block and the Bayan Har block. The response pattern of the rock mass to the loading provides insights into the movement of faults. The mechanical test results indicate that during quasi-hydrostatic loading of granite and sandstone, the volume expansion of granite and sandstone becomes more obvious as the strain rate increases [81], showing a positive correlation between the strain rate and rock damage [82]. The XSHF is located in an area comprising granite and sandstone lithologies, and the numerical inversion results reveal that the SW wall experiences a high strain rate environment, whereas the strain rate decreases rapidly from west to east on the NE wall [43,83]. This suggests that the stronger activity of the SW wall has caused a wider rock damage zone in the study area. In the context of the India–Asia collision, the Sichuan–Yunnan block, i.e., the SW wall, acts as a driving wall, resulting in the width of the damage zones of the SW wall being generally wider than those of the NE wall.

5. Conclusions

The XSHF is the boundary fault located in the southeastern margin of the Tibetan Plateau and was formed due to the India–Asia collision. The SW wall and NE wall are surrounded by damage zones with widths of approximately 20.8 km and 17.1 km, respectively. Observations of the rock structure around the XSHF show that the damage zones in the two walls follow a negative power-law decay trend, but the distribution of the fracture frequency and rock strength in the different damage zones in the two walls is inconsistent, that is, the width of damage zone of the TDZ is larger than that of the LDZ and WDZ. Combined with previous studies, this shows that the decay parameter is highly influenced by the displacement if the displacement is smaller than hundreds of meters; however, but the decay parameter tends to stabilize at large displacement scales (larger than hundreds of meters), the width of the damage zone shows a negative power-law correlation with slip displacement, and the expansion rate of the damage zone slows down with the increase in slip displacement. Finally, we conclude that the differences in rock damage characteristics among different damage zones in the XSHF are mainly caused by the inconsistent stress distribution in different damage zones caused by tectonic movement.

The asymmetric distribution of the damage zones across the fault is mainly attributed to the differences in activity rates between the blocks on both walls of the fault.

Supplementary Materials: The following supporting information can be downloaded at: <https://www.mdpi.com/article/10.3390/app14062439/s1>, Table S1: Exposed bedrock parameters of LHS tip; Table S2: Exposed bedrock parameters of QNS; Table S3: Exposed bedrock parameters of DFS; Table S4: Exposed bedrock parameters of DFS; Table S5: Exposed bedrock parameters of KDS.

Author Contributions: Conceptualization, J.L., S.G. and S.Q.; methodology, S.G., J.L. and S.Q.; formal analysis, J.L., S.G. and Q.W.; investigation, S.G., J.L., Q.W., B.Z., Y.Z. (Yu Zou), Y.L. and X.L.; resources, J.L., S.G., Q.W., B.Z., Y.L. and X.L.; data curation, J.L. and S.G.; writing—original draft preparation, J.L., S.G. and S.Q., writing—review and editing, J.L., S.G., S.Q., B.Z., Y.Z. (Yu Zou), and K. Z.; visualization J.L., S.G. and Q.W.; supervision, S.Q.; project administration, S.G., B.Z., J.L., Y.Z. (Yu Zou) and Y.Z. (Yaguo Zhang); funding acquisition, S.G. and S.Q.; All authors have read and agreed to the published version of the manuscript.

Funding: This research was funded by National Natural Science Foundation of China (42077266, 41825018), the Second Tibetan Plateau Scientific Expedition and Research Program (2019QZKK0904), the National Key Research and Development Program of China (2023YFC3012004-05), and the Youth Innovation Promotion Association of the Chinese Academy of Sciences (2022062).

Institutional Review Board Statement: Not applicable.

Informed Consent Statement: Not applicable.

Data Availability Statement: Data are contained within the article and Supplementary Materials, further inquiries can be directed to the corresponding author.

Conflicts of Interest: The authors declare no conflicts of interest.

References

- Kim, Y.; Peacock, D.; Sanderson, D.J. Fault damage zones. *J. Struct. Geol.* **2004**, *26*, 503–517. [[CrossRef](#)]
- Caine, J.; Evans, J.; Forster, C. Fault zone architecture and permeability structure. *Geology* **1996**, *24*, 1025–1028. [[CrossRef](#)]
- Odling, N.E.; Harris, S.D.; Knipe, R.J. Permeability scaling properties of fault damage zones in siliclastic rocks. *J. Struct. Geol.* **2004**, *26*, 1727–1747. [[CrossRef](#)]
- Choi, J.H.; Edwards, P.; Ko, K.; Kim, Y.S. Definition and classification of fault damage zones: A review and a new methodological approach. *Earth-Sci. Rev.* **2016**, *152*, 70–87. [[CrossRef](#)]
- Peacock, D.C.P.; Dimmen, V.; Rotevatn, A.; Sanderson, D.J. A broader classification of damage zones. *J. Struct. Geol.* **2017**, *102*, 179–192. [[CrossRef](#)]
- Scholz, C.H.; Cowie, P.A. Determination of total strain from faulting using slip measurements. *Nature* **1990**, *346*, 837–839. [[CrossRef](#)]
- Bedford, J.D.; Faulkner, D.R.; Lapusta, N. Fault rock heterogeneity can produce fault weakness and reduce fault stability. *Nat. Commun.* **2022**, *13*, 326. [[CrossRef](#)]
- Mizoguchi, K.; Ueta, K. Microfractures within the fault damage zone record the history of fault activity. *Geophys. Res. Lett.* **2013**, *40*, 2023–2027. [[CrossRef](#)]
- Celestino, M.A.L.; de Miranda, T.S.; Mariano, G.; de Lima Alencar, M.; de Carvalho, B.R.B.M.; da Cruz Falcão, T.; Topan, J.A.; Barbosa, J.A.; Gomes, I.F. Fault damage zones width: Implications for the tectonic evolution of the northern border of the Araripe Basin, Brazil, NE Brazil. *J. Struct. Geol.* **2020**, *138*, 104116. [[CrossRef](#)]
- Valoroso, L.; Chiaraluce, L.; Collettini, C. Earthquakes and fault zone structure. *Geology* **2014**, *42*, 343–346. [[CrossRef](#)]
- Thakur, P.; Huang, Y.; Kaneko, Y. Effects of low-velocity fault damage zones on long-term earthquake behaviors on mature strike-slip faults. *J. Geophys. Res. Solid Earth* **2020**, *125*, e2020JB019587. [[CrossRef](#)]
- Wu, G.; Gao, L.; Zhang, Y.; Ning, C.; Xie, E. Fracture attributes in reservoir-scale carbonate fault damage zones and implications for damage zone width and growth in the deep subsurface. *J. Struct. Geol.* **2019**, *118*, 181–193. [[CrossRef](#)]
- Dockrill, B.; Shipton, Z.K. Structural controls on leakage from a natural CO₂ geologic storage site: Central Utah, USA. *J. Struct. Geol.* **2010**, *32*, 1768–1782. [[CrossRef](#)]
- Cappa, F.; Rutqvist, J. Impact of CO₂ geological sequestration on the nucleation of earthquakes. *Geophys. Res. Lett.* **2011**, *38*, L17313. [[CrossRef](#)]
- Faulkner, D.R.; Mitchell, T.M.; Healy, D.; Heap, M.J. Slip on weak faults by the rotation of regional stress in the fracture damage zone. *Nature* **2006**, *444*, 922–925. [[CrossRef](#)]
- Zhang, S.; Ma, X. How does in situ stress rotate within a fault zone? Insights from explicit modeling of the frictional, fractured rock mass. *J. Geophys. Res. Solid Earth* **2021**, *126*, e2021JB022348. [[CrossRef](#)]

17. Faulkner, D.R.; Lewis, A.C.; Rutter, E.H. On the internal structure and mechanics of large strike-slip fault zones: Field observations of the Carboneras fault in southeastern Spain. *Tectonophysics* **2003**, *367*, 235–251. [[CrossRef](#)]
18. De Jousseineau, G.; Aydin, A. The evolution of the damage zone with fault growth in sandstone and its multiscale characteristics. *J. Geophys. Res. Solid Earth* **2007**, *112*, B12401. [[CrossRef](#)]
19. Ma, D.; Wu, G.; Scarselli, N.; Luo, X.; Han, J.; Chen, Z. Seismic damage zone and width–throw scaling along the strike-slip faults in the Ordovician carbonates in the Tarim Basin. *Pet. Sci.* **2019**, *16*, 752–762. [[CrossRef](#)]
20. Scholz, C.H.; Anders, M. The permeability of faults. In *The Mechanical Involvement of Fluids in Faulting*; US Department of the Interior, Geological Survey: Reston, VA, USA, 1994; pp. 94–228.
21. Torabi, A.; Berg, S.S. Scaling of fault attributes: A review. *Mar. Pet. Geol.* **2011**, *28*, 1444–1460. [[CrossRef](#)]
22. Lei, G.; Yang, C.; Wang, G.; Chen, S.; Wei, X.; Huo, L. The Development Law and Mechanical Causes of Fault Influenced Zone. *Chin. J. Rock Mech. Eng.* **2016**, *35*, 231–241, (In Chinese with English Abstract).
23. Torabi, A.; Ellingsen, T.S.S.; Johannessen, M.U.; Alaei, B.; Rotevatn, A.; Chiarella, D. Fault zone architecture and its scaling laws: Where does the damage zone start and stop? *Geol. Soc. Lond. Spec. Publ.* **2020**, *496*, 99–124. [[CrossRef](#)]
24. Gudmundsson, A.; Simmenes, T.H.; Larsen, B.; Philipp, S.L. Effects of internal structure and local stresses on fracture propagation, deflection, and arrest in fault zones. *J. Struct. Geol.* **2010**, *32*, 1643–1655. [[CrossRef](#)]
25. Schueller, S.; Braathen, A.; Fossen, H.; Tveranger, J. Spatial distribution of deformation bands in damage zones of extensional faults in porous sandstones: Statistical analysis of field data. *J. Struct. Geol.* **2013**, *52*, 148–162. [[CrossRef](#)]
26. Tapponnier, P.; Molnar, P. Active faulting and tectonics in China. *J. Geophys. Res.* **1977**, *82*, 2905–2930. [[CrossRef](#)]
27. Zhang, P.Z. A review on active tectonics and deep crustal processes of the Western Sichuan region, eastern margin of the Tibetan Plateau. *Tectonophysics* **2013**, *584*, 7–22. [[CrossRef](#)]
28. Roy, S.G.; Tucker, G.E.; Koons, P.O.; Smith, S.M.; Upton, P.A. Fault Runs through it: Modeling the influence of rock strength and grain-size distribution in a fault-damaged landscape. *J. Geophys. Res. Earth Surf.* **2016**, *121*, 1911–1930. [[CrossRef](#)]
29. Wang, X.; Crosta, G.B.; Clague, J.J.; Stead, D.; Sun, J.; Qi, S.; Liu, H. Fault controls on spatial variation of fracture density and rock mass strength within the Yarlung Tsangpo Fault damage zone (southeastern Tibet). *Eng. Geol.* **2021**, *291*, 106238. [[CrossRef](#)]
30. Allen, C.R.; Luo, Z.; Qian, H.; Wen, X.; Zhou, H.; Huang, W. Field study of a highly active fault zone: The Xianshuihe fault of southwestern China. *Geol. Soc. Am. Bull.* **1991**, *103*, 1178–1199. [[CrossRef](#)]
31. Jackson, W.T., Jr.; Robinson, D.M.; Weislogel, A.L.; Jian, X. Cenozoic reactivation along the late Triassic Ganzi-Litang suture, eastern Tibetan plateau. *Geosci. Front.* **2020**, *11*, 1069–1080. [[CrossRef](#)]
32. Li, B.; Jia, C.; Pang, X.; Guan, S.; Yang, G.; Shi, X.; Li, C. The spatial distribution of the foreland thrust tectonic deformation in the Circum-Tibetan Plateau Basin and range system. *Acta Geol. Sin.* **2007**, *2007*, 1200–1207, (In Chinese with English Abstract).
33. Molnar, P.; England, P.; Martinod, J. Mantle dynamics, uplift of the Tibet Plateau, and the Indian monsoon. *Rev. Geophys.* **1993**, *31*, 357–396. [[CrossRef](#)]
34. Wang, S.; Fan, C.; Wang, G.; Wang, E. Late Cenozoic deformation along the northwestern continuation of the Xianshuihe fault system, Eastern Tibetan Plateau. *Geol. Soc. Am. Bull.* **2008**, *120*, 312–327. [[CrossRef](#)]
35. Clark, M.K.; Royden, L.H. Topographic ooze: Building the eastern margin of Tibet by lower crustal flow. *Geology* **2000**, *28*, 703–706. [[CrossRef](#)]
36. Royden, L.H.; Burchfiel, B.C.; King, R.W.; Wang, E.; Chen, Z.; Shen, F.; Liu, Y. Surface deformation and lower crustal flow in eastern Tibet. *Science* **1997**, *276*, 788–790. [[CrossRef](#)]
37. Tapponnier, P.; Zhiqin, X.; Roger, F.; Meyer, B.; Arnaud, N.; Wittlinger, G.; Jingsui, Y. Oblique stepwise rise and growth of the Tibet Plateau. *Science* **2001**, *294*, 1671–1677. [[CrossRef](#)]
38. Zhang, Q.W.; Zhang, P.Z.; Wang, C.; Wang, Y.P.; Ellis, M.A. Earthquake triggering and delaying caused by fault interaction on Xianshuihe fault belt, southwestern China. *Acta Seismol. Sin.* **2003**, *16*, 156–165. [[CrossRef](#)]
39. Wen, X.; Ma, S.; Xu, X.; He, Y. Historical pattern and behavior of earthquake ruptures along the eastern boundary of the Sichuan-Yunnan faulted-block, southwestern China. *Phys. Earth Planet. Inter.* **2008**, *168*, 16–36. [[CrossRef](#)]
40. Bai, M.; Chevalier, M.L.; Pan, J.; Replumaz, A.; Leloup, P.H.; Métois, M.; Li, H. Southeastward increase of the late Quaternary slip-rate of the Xianshuihe fault, eastern Tibet. Geodynamic and seismic hazard implications. *Earth Planet. Sci. Lett.* **2018**, *485*, 19–31. [[CrossRef](#)]
41. Yin, A.; Harrison, T.M. Geologic evolution of the Himalayan-Tibetan orogen. *Annu. Rev. Earth Planet. Sci.* **2000**, *28*, 211–280. [[CrossRef](#)]
42. Osmundsen, P.T.; Henderson, I.; Lauknes, T.R.; Larsen, Y.; Redfield, T.F.; Dehls, J. Active normal fault control on landscape and rock-slope failure in northern Norway. *Geology* **2009**, *37*, 135–138. [[CrossRef](#)]
43. Li, Y.; Liu, M.; Li, Y.; Chen, L. Active crustal deformation in southeastern Tibetan Plateau: The kinematics and dynamics. *Earth Planet. Sci. Lett.* **2019**, *523*, 115708. [[CrossRef](#)]
44. Qiao, X.; Zhou, Y. Geodetic imaging of shallow creep along the Xianshuihe fault and its frictional properties. *Earth Planet. Sci. Lett.* **2021**, *567*, 117001. [[CrossRef](#)]
45. Qi, S.W. *Engineering Geological Petrofabric Database of Qinghai Tibet Plateau*; A Big Earth Data Platform for Three Poles: Lanzhou, China, 2021. [[CrossRef](#)]

46. Faulkner, D.R.; Jackson, C.A.L.; Lunn, R.J.; Schlische, R.W.; Shipton, Z.K.; Wibberley, C.A.J.; Withjack, M.O. A review of recent developments concerning the structure, mechanics and fluid flow properties of fault zones. *J. Struct. Geol.* **2010**, *32*, 1557–1575. [[CrossRef](#)]
47. Palmstrom, A. Measurements of and correlations between block size and rock quality designation (RQD). *Tunn. Undergr. Space Technol.* **2005**, *20*, 362–377. [[CrossRef](#)]
48. Love, A.E.H. *A Treatise on the Mathematical Theory of Elasticity*; Cambridge University Press: Cambridge, UK, 2013.
49. Aydin, A.; Basu, A. The Schmidt hammer in rock material characterization. *Eng. Geol.* **2005**, *81*, 1–14. [[CrossRef](#)]
50. Savage, H.M.; Shreedharan, S.; Fagereng, Å.; Morgan, J.K.; Meneghini, F.; Wang, M.; McNamara, D.D.; Wallace, L.M.; Saffer, D.M.; Barnes, P.M.; et al. Asymmetric brittle deformation at the Pāpaku fault, Hikurangi subduction margin, NZ, IODP Expedition 375. *Geochem. Geophys. Geosyst.* **2021**, *22*, e2021GC009662. [[CrossRef](#)]
51. Ostermeijer, G.A.; Mitchell, T.M.; Aben, F.M.; Dorsey, M.T.; Browning, J.; Rockwell, T.K.; Fletcher, J.M.; Ostermeijer, F. Damage zone heterogeneity on seismogenic faults in crystalline rock; a field study of the Borrego Fault, Baja California. *J. Struct. Geol.* **2020**, *137*, 104016. [[CrossRef](#)]
52. Chen, G.; Xu, X.; Wen, X.; Chen, Y. Late Quaternary slip-rates and slip partitioning on the southeastern Xianshuihe fault system, eastern Tibetan Plateau. *Acta Geol. Sin.* **2016**, *90*, 537–554.
53. Bai, M.; Chevalier, M.L.; Leloup, P.H.; Li, H.; Pan, J.; Replumaz, A.; Wang, S.; Li, K.; Wu, Q.; Liu, F.; et al. Spatial slip rate distribution along the SE Xianshuihe fault, eastern Tibet, and earthquake hazard assessment. *Tectonics* **2021**, *40*, e2021TC006985. [[CrossRef](#)]
54. Shipton, Z.K.; Cowie, P.A. Damage zone and slip-surface evolution over μm to km scales in high-porosity Navajo sandstone, Utah. *J. Struct. Geol.* **2001**, *23*, 1825–1844. [[CrossRef](#)]
55. French, M.E.; Morgan, J.K. Pore fluid pressures and strength contrasts maintain frontal fault activity, northern Hikurangi margin, New Zealand. *Geophys. Res. Lett.* **2020**, *47*, e2020GL089209. [[CrossRef](#)]
56. Templeton, E.L.; Rice, J.R. Off-fault plasticity and earthquake rupture dynamics: 1. Dry materials or neglect of fluid pressure changes. *J. Geophys. Res. Solid Earth* **2008**, *113*, B09306. [[CrossRef](#)]
57. Lin, A.; Yamashita, K. Spatial variations in damage zone width along strike-slip faults: An example from active faults in southwest Japan. *J. Struct. Geol.* **2013**, *57*, 1–15. [[CrossRef](#)]
58. Keren, T.T.; Kirkpatrick, J.D. The damage is done: Low fault friction recorded in the damage zone of the shallow Japan Trench décollement. *J. Geophys. Res. Solid Earth* **2016**, *121*, 3804–3824. [[CrossRef](#)]
59. Savage, H.M.; Brodsky, E.E. Collateral damage: Evolution with displacement of fracture distribution and secondary fault strands in fault damage zones. *J. Geophys. Res. Solid Earth* **2011**, *116*, B03405. [[CrossRef](#)]
60. Beach, A.; Welbon, A.I.; Brockbank, P.J.; McCallum, J. Reservoir damage around faults; outcrop examples from the Suez Rift. *Pet. Geosci.* **1999**, *5*, 109–116. [[CrossRef](#)]
61. Mayolle, S.; Soliva, R.; Caniven, Y.; Wibberley, C.; Ballas, G.; Milesi, G.; Dominguez, S. Scaling of fault damage zones in carbonate rocks. *J. Struct. Geol.* **2019**, *124*, 35–50. [[CrossRef](#)]
62. Fossen, H.; Hesthammer, J. Possible absence of small faults in the Gullfaks Field, northern North Sea: Implications for downscaling of faults in some porous sandstones. *J. Struct. Geol.* **2000**, *22*, 851–863. [[CrossRef](#)]
63. Wilson, J.E.; Chester, J.S.; Chester, F.M. Microfracture analysis of fault growth and wear processes, Punchbowl Fault, San Andreas system, California. *J. Struct. Geol.* **2003**, *25*, 1855–1873. [[CrossRef](#)]
64. Mitchell, T.M.; Faulkner, D.R. The nature and origin of off-fault damage surrounding strike-slip fault zones with a wide range of displacements: A field study from the Atacama fault system, northern Chile. *J. Struct. Geol.* **2009**, *31*, 802–816. [[CrossRef](#)]
65. Faulkner, D.R.; Mitchell, T.M.; Jensen, E.; Cembrano, J. Scaling of fault damage zones with displacement and the implications for fault growth processes. *J. Geophys. Res. Solid Earth* **2011**, *116*, B05403. [[CrossRef](#)]
66. Childs, C.; Manzocchi, T.; Walsh, J.J.; Bonson, C.G.; Nicol, A.; Schöpfer, M.P. A geometric model of fault zone and fault rock thickness variations. *J. Struct. Geol.* **2009**, *31*, 117–127. [[CrossRef](#)]
67. McKay, L.; Lunn, R.J.; Shipton, Z.K.; Pytharouli, S.; Roberts, J.J. Do intraplate and plate boundary fault systems evolve in a similar way with repeated slip events? *Earth Planet. Sci. Lett.* **2021**, *559*, 116757. [[CrossRef](#)]
68. Pakzad, R.; Wang, S.; Sloan, S.W. Three-dimensional finite element simulation of fracture propagation in rock specimens with pre-existing fissure(s) under compression and their strength analysis. *Int. J. Numer. Anal. Methods Geomech.* **2020**, *44*, 1472–1494. [[CrossRef](#)]
69. Chen, T.; Foulger, G.R.; Mathias, S.A.; Gong, B. Numerical investigation on origin and evolution of polygonal cracks on rock surfaces. *Eng. Geol.* **2022**, *311*, 106913. [[CrossRef](#)]
70. Guo, S.; Qi, S. Numerical study on progressive failure of hard rock samples with an unfilled undulate joint. *Eng. Geol.* **2015**, *193*, 173–182. [[CrossRef](#)]
71. Guo, S.; Qi, S.; Cai, M. Influence of tunnel wall roughness and localized stress concentrations on the initiation of brittle spalling. *Bull. Eng. Geol. Environ.* **2016**, *75*, 1597–1607. [[CrossRef](#)]
72. Luo, G.; Qi, S.; Zheng, B. Rate effect on the direct shear behavior of granite rock bridges at low to subseismic shear rates. *J. Geophys. Res. Solid Earth* **2022**, *127*, e2022JB024348. [[CrossRef](#)]
73. Guo, S.; Qi, S.; Zhan, Z.; Ma, L.; Gure, E.G.; Zhang, S. Numerical study on the progressive failure of heterogeneous geomaterials under varied confining stresses. *Eng. Geol.* **2020**, *269*, 105556. [[CrossRef](#)]

74. Xie, H.; Lu, J.; Li, C.; Li, M.; Gao, M. Experimental study on the mechanical and failure behaviors of deep rock subjected to true triaxial stress: A review. *Int. J. Min. Sci. Technol.* **2022**, *32*, 915–950. [[CrossRef](#)]
75. Aarland, R.K.; Skjerven, J. Fault and fracture characteristics of a major fault zone in the northern North Sea: Analysis of 3D seismic and oriented cores in the Brage Field (Block 31/4). *Geol. Soc. Lond. Spec. Publ.* **1998**, *127*, 209–229. [[CrossRef](#)]
76. Ma, S.; Zeng, L.; Tian, H.; Shi, X.; Wu, W.; Yang, S.; Luo, L.; Xu, X. Fault damage zone and its effect on deep shale gas: Insights from 3D seismic interpretation in the southern Sichuan Basin, China. *J. Struct. Geol.* **2023**, *170*, 104848. [[CrossRef](#)]
77. Boncio, P.; Liberi, F.; Caldarella, M.; Nurminen, F.C. Width of surface rupture zone for thrust earthquakes: Implications for earthquake fault zoning. *Nat. Hazards Earth Syst. Sci.* **2018**, *18*, 241–256. [[CrossRef](#)]
78. Sylvester, A.G. Strike-slip faults. *Geol. Soc. Am. Bull.* **1988**, *100*, 1666–1703. [[CrossRef](#)]
79. Burchfiel, B.C.; Zhiliang, C.; Yupinc, L.; Royden, L.H. Tectonics of the Longmen Shan and adjacent regions, central China. *Int. Geol. Rev.* **1995**, *37*, 661–735. [[CrossRef](#)]
80. Burchfiel, B.C.; Royden, L.H.; Van der Hilst, R.D.; Hager, B.H.; Chen, Z.; King, R.W.; Li, C.; Lü, J.; Yao, H.; Kirby, E. A geological and geophysical context for the Wenchuan earthquake of 12 May 2008, Sichuan, People's Republic of China. *GSA Today* **2008**, *18*, 4–11. [[CrossRef](#)]
81. Xu, R.; Zhang, S.; Li, Z.; Yan, X. Experimental investigation of the strain rate effect on crack initiation and crack damage thresholds of hard rock under quasi-static compression. *Acta Geotech.* **2023**, *18*, 903–920. [[CrossRef](#)]
82. Earle, S. *Physical Geology*; BCcampus: Victoria, BC, Canada, 2015; pp. 337–339.
83. Copley, A. Kinematics and dynamics of the southeastern margin of the Tibetan Plateau. *Geophys. J. Int.* **2008**, *174*, 1081–1100. [[CrossRef](#)]

Disclaimer/Publisher's Note: The statements, opinions and data contained in all publications are solely those of the individual author(s) and contributor(s) and not of MDPI and/or the editor(s). MDPI and/or the editor(s) disclaim responsibility for any injury to people or property resulting from any ideas, methods, instructions or products referred to in the content.